Supplementary Information for: Time-resolved momentum imaging of UV photodynamics in structural isomers of iodopropane probed by site-selective XUV ionization

Felix Allum,[1,2,3,*] Yoshiaki Kumagai,[4] Kiyonobu Nagaya,[5] James Harries,[6] Hiroshi Iwayama,[7,8] Mathew Britton,[1] Philip H. Bucksbaum,[1] Michael Burt,[9] Mark Brouard,[9] Briony Downes-Ward,[10] Taran Driver,[2] David Heathcote,[9] Paul Hockett,[11] Andrew J. Howard,[1] Jason W. L. Lee,[12] Yusong Liu,[1] Edwin Kukk,[13] Joseph W. McManus,[9] Dennis Milsesevic,[9] Akinobu Niozu,[14] Johannes Niskannen,[13] Andrew Orr-Ewing,[15] Shigeki Owada,[16,17] Patrick Robertson,[9] Artem Rudenko,[18] Kiyoshi Ueda,[19] James Unwin,[9] Claire Vallance,[9] Tiffany Walmsley,[9] Russell S. Minns,[10] Daniel Rolles,[18] Michael N. R. Ashfold,[15] and Ruaridh Forbes[2,20,†]

[1] *PULSE Institute, SLAC National Accelerator Laboratory, 2575 Sand Hill Road, Menlo Park, CA 94025, USA*
[2] *Linac Coherent Light Source, SLAC National Accelerator Laboratory, 2575 Sand Hill Road, Menlo Park, CA 94025, USA*
[3] *Deutsches Elektronen-Synchrotron DESY, Notkestraße85, 22607 Hamburg, Germany*
[4] *Department of Applied Physics, Tokyo University of Agriculture and Technology, Tokyo, Japan*
[5] *Department of Physics, Kyoto University, Kyoto 606-8502, Japan*
[6] *QST, SPring-8, Kouto 1-1-1, Sayo, Hyogo, Japan*
[7] *Institute for Molecular Science, Okazaki 444-8585, Japan*
[8] *Sokendai (The Graduate University for Advanced Studies), Okazaki 444-8585, Japan*
[9] *Chemistry Research Laboratory, Department of Chemistry, University of Oxford, Oxford OX1 3TA, United Kingdom*
[10] *Chemistry, University of Southampton, Highfield, Southampton SO17 1BJ, United Kingdom*
[11] *National Research Council of Canada, 100 Sussex Dr. Ottawa, ON K1A 0R6, Canada*
[12] *Deutsches Elektronen-Synchrotron DESY, Hamburg, Germany*
[13] *Department of Physics and Astronomy, University of Turku, FI-20014 Turku, Finland*
[14] *Graduate School of Advanced Science and Engineering, Hiroshima University, Higashi-Hiroshima 739-8526, Japan*
[15] *School of Chemistry, University of Bristol, Cantock's Close, Bristol BS8 1TS, UK*
[16] *RIKEN SPring-8 Center, Sayo, Hyogo, 679-5148, Japan*
[17] *Japan Synchrotron Radiation Research Institute, Hyogo, Japan*
[18] *J.R. Macdonald Laboratory, Department of Physics, Kansas State University, Manhattan, Kansas 66506, USA*
[19] *Department of Chemistry, Tohoku University, Sendai 980-8578, Japan*
[20] *Department of Chemistry, University of California, Davis, California 95616, USA.*

(Dated: July 11, 2025)

I. DELAY-DEPENDENT ION MOMENTUM DISTRIBUTIONS

Figure 1 of the main manuscript shows delay-dependent ion momentum distributions following subtracting of averaged UV-late data. Fig S1 presents the equivalent data without any background subtraction. As can be seen, probe-only signal present at all delays is only significant in the I^{2+} ion. For higher iodine charge states, there is limited ion production (particularly in the <300 a.u. momentum region) in the probe-only (or UV-late) case.

Figure S2 presents the same data as Fig. S1, but zoomed into low ion momentum and pump-probe delays close to time-zero. This is to highlight the delay-dependent shifts of low momentum (Channel II) ions from 1-IP as a function of pump-probe delay, as discussed in the main text.

Figure S3 displays delay-dependent momentum distributions associated with Channel II plotted as a series of lineouts, again to show delay-dependent shifts present in 1-IP in another representation.

Figure 3 of the main text compares the asymptotic KER distribution of Channel II ions from I^{4+} to literature measurements of the KER distributions associated with photodissociation in 1-/2-IP [1, 2]. While the I^{4+} ion was chosen for this comparison, we would expect to see the same asymptotic KER distribution in this channel for each ion, as the KER of these ions should be determined solely by the UV-induced photodissociation. These KER distributions

* felix.allum@desy.de
† ruforbes@stanford.edu

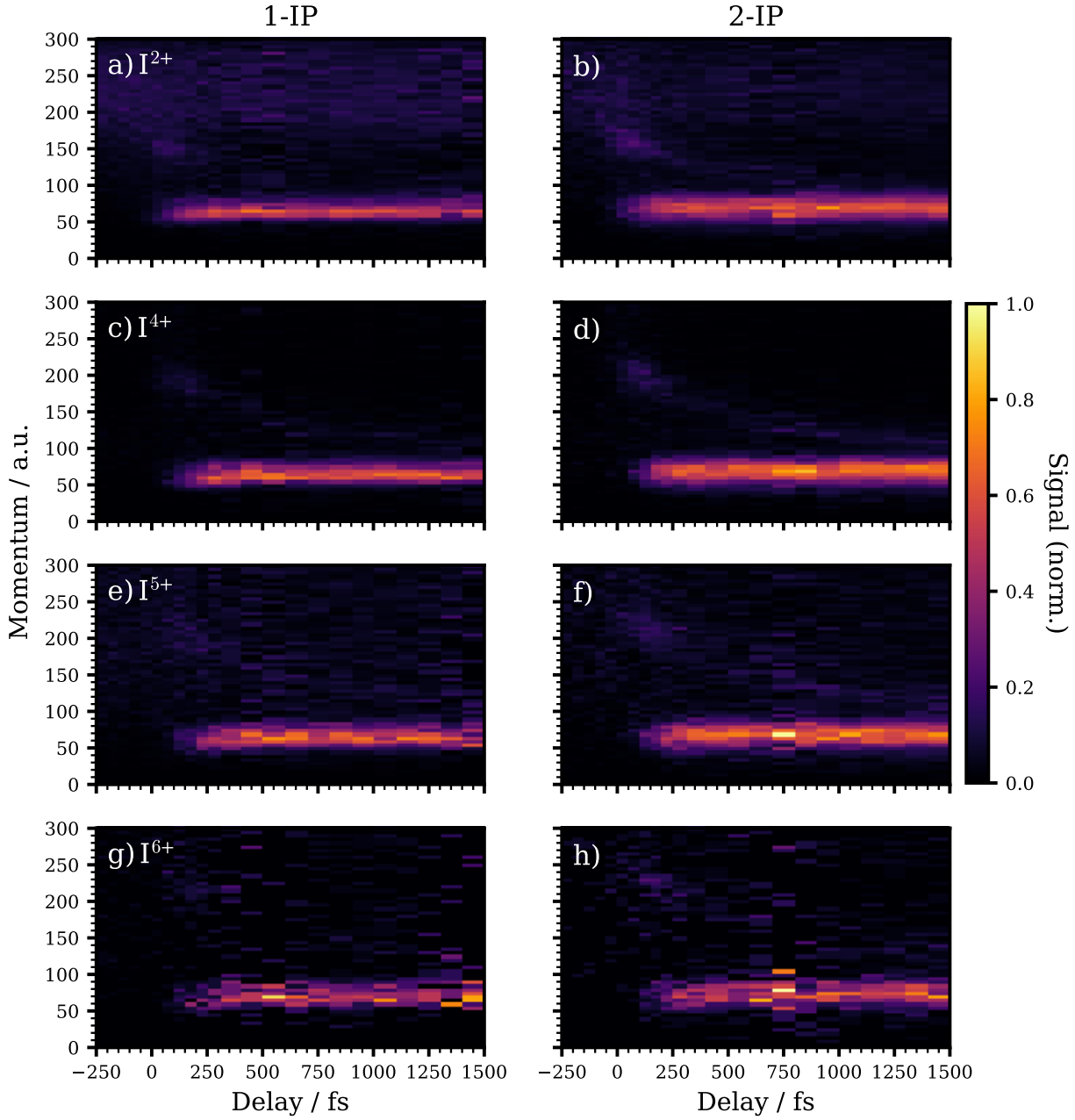

FIG. S1. Comparison of delay-dependent momentum (in atomic units of momentum, a.u.) distributions for I^{n+} ions (n=2,4,5,6), where positive delays corresponds to the UV pump arriving before the XUV probe, and vice versa. Data for each charge state are plotted on individually-normalised colour scales. No background subtracting has been applied to these data.

for each iodine charge state from both isomers are compared in S4. As expected, there is very little difference between the iodine charge states. The I^{6+} ion appears to be a slight outlier, particularly in 1-IP, but this is, at least partly, due to the relatively low statistics in this ion.

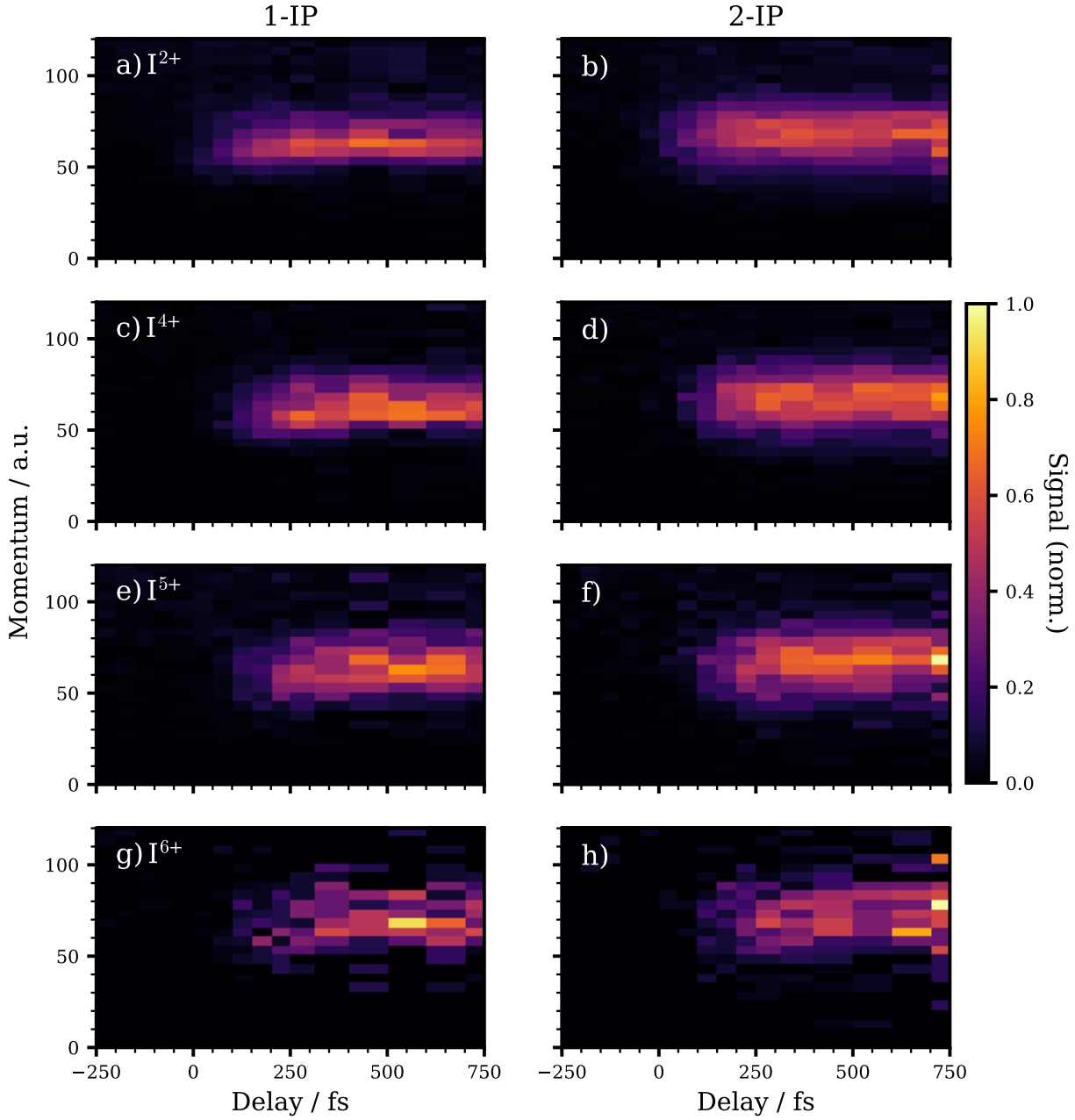

FIG. S2. Comparison of delay-dependent momentum (in atomic units of momentum, a.u.) distributions for I^{n+} ions (n=2,4,5,6), where positive delays corresponds to the UV pump arriving before the XUV probe, and vice versa. Data for each charge state are plotted on individually-normalised colour scales. No background subtracting has been applied to these data. These plots have been zoomed in to low absolute momentum and short pump-probe delays, to better highlight the delay-dependent momentum of Channel II ions in 1-IP.

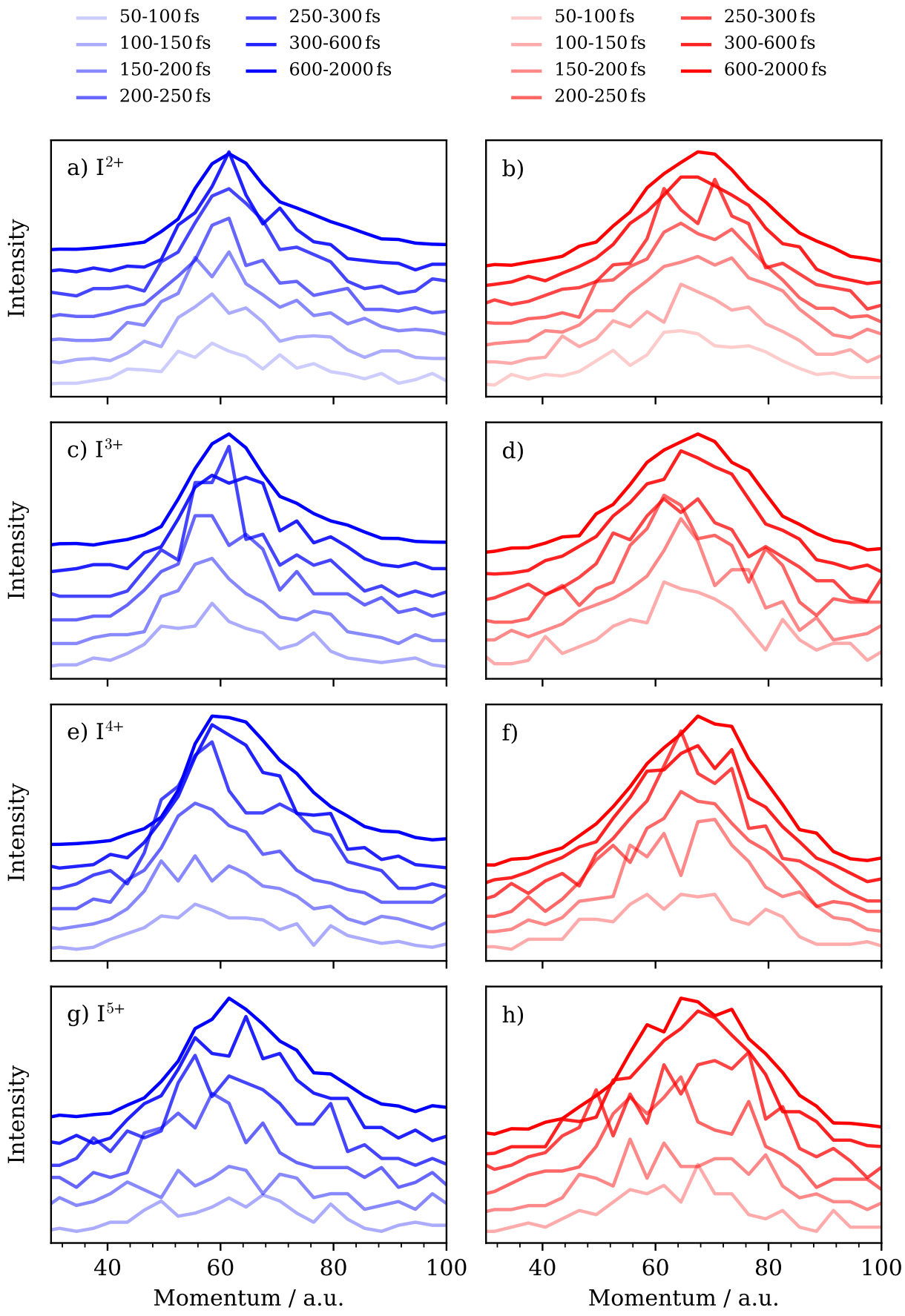

FIG. S3. Comparison of delay-dependent momentum (in atomic units of momentum, a.u.) distributions for I^{n+} ions (n=2,3,4,5), focussing on the Channel II feature at early pump-probe delays. Data for different pump-probe delay bins are individually plotted and colour-coded as labelled.

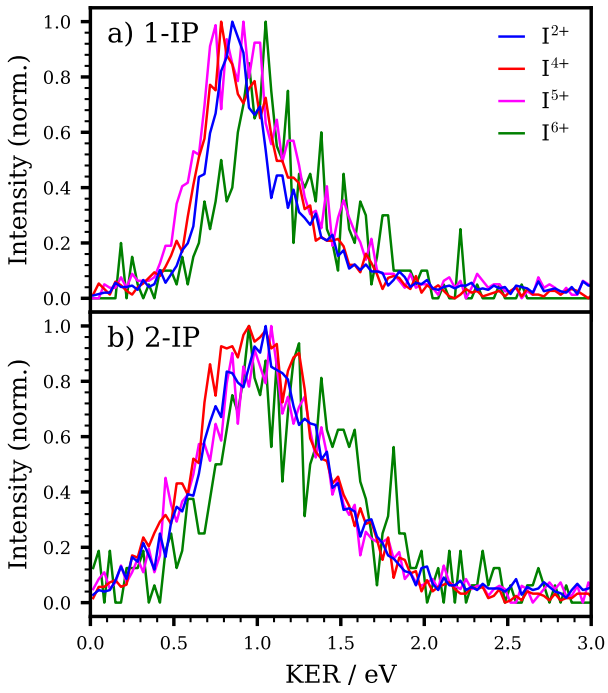

FIG. S4. Comparison of asymptotic KER distributions for Channel II I^{n+} ions (n=2,4,5,6) from 1- and 2-IP, obtained by integrating data between pump-probe delays of +300 fs and +1000 fs. Equivalent data for the I^{4+} case is shown in Fig. 3 of the main text.

II. CHARGE TRANSFER DYNAMICS

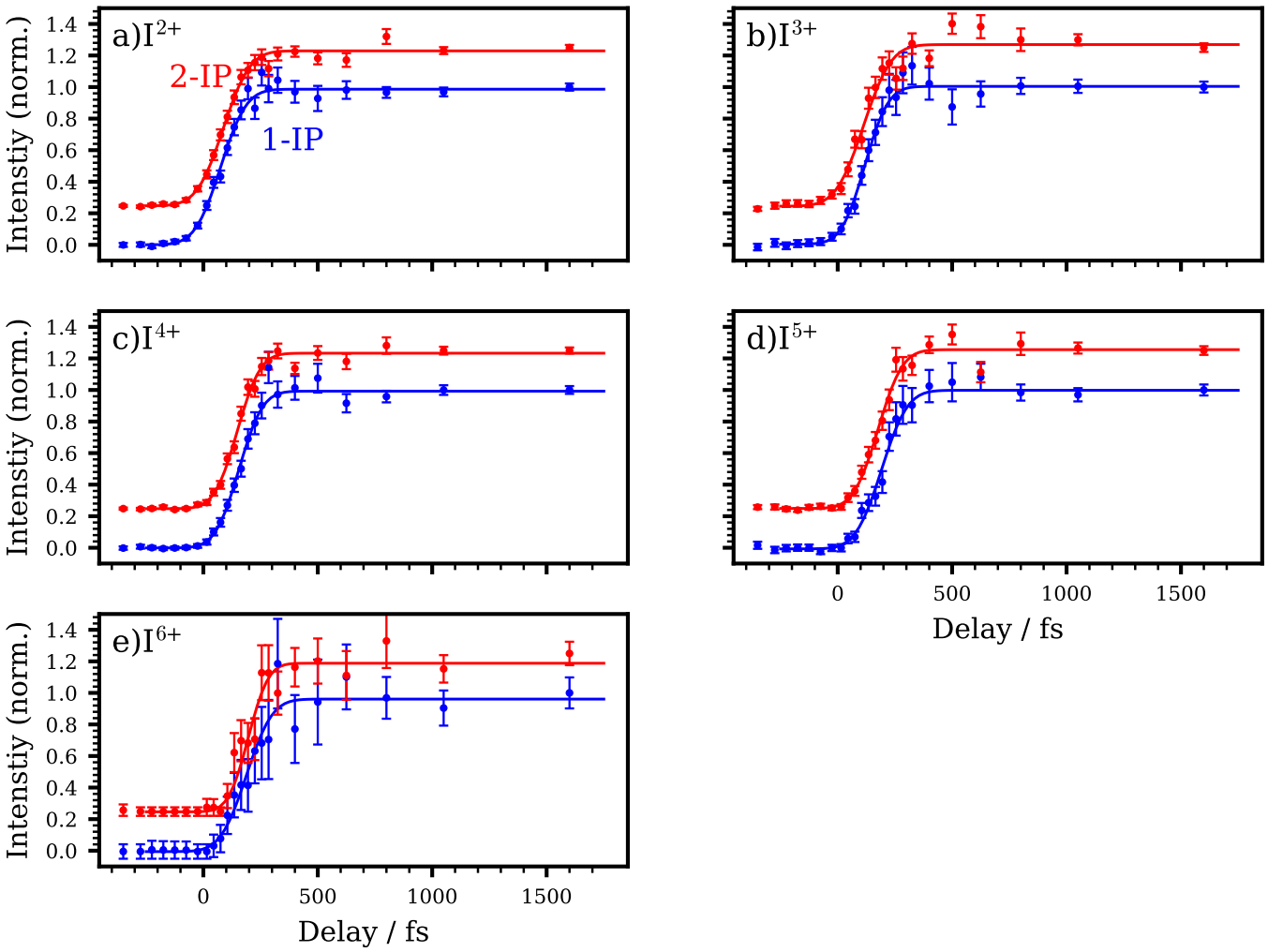

FIG. S5. Delay-dependent yields of low-momenta (40 a.u.<p<90 a.u.) I^{n+} (n=2-6) ions from 1-IP (blue) and 2-IP (red). As in Figure 4a) of the main manuscript, the data for 2-IP and 1-IP are vertically offset for visual clarity.

Figure 4a) of the main text shows the delay-dependent counts of low momentum (Channel II) I^{4+} ions from 1-IP and 2-IP, alongside fits to the experimental data using a normal CDF. Figure S6 shows the equivalent data for all I^{n+} charge states (n=2-5). In all cases, a fairly sharp increase in intensity is observed shortly after time-zero, and this increase is well captured by the CDF fits.

As discussed in the main text, we choose to analyze the centres of the CDF fits relative to the fitted centre for the I^{2+} ion. As adopted in previous work [3], this is in order to negate ambiguity regarding the precise assignment of time-zero, which has an associated uncertainty and may not be exactly the same between the data collected for the two isomers. Figure S7 presents the fitted centres without such shifting. It can be seen that the fitted centres are similar between the two isomers, with the I^{2+} yield rising at slightly earlier delays in 1-IP than 2-IP. There is, however, a ∼30-40 fs offset between the experimental data and the predictions from the OTB model. Without a more reliable way to determine time-zero from the experimental data it is difficult to comment whether this offset comes from a slight error in the assignment of time-zero or due to deviations in the true CT behaviour from that predicted by the simple modelling.

Our previous work on 2-IP [4] focussed on signal arising from CT and subsequent Coulombic repulsion at early pump-probe delays (Channel I). As mentioned in the main text, the momentum distributions associated with this feature appear to be laregely isomer independent. This can be seen in Figure S5, which compares Channel I momentum distributions from 1-IP and 2-IP for each iodine ion charge state. Within experimental uncertainty there are no substantial differences. In the I^{2+} (and perhaps I^{4+}) case it appears that the ions from 2-IP case have a slightly

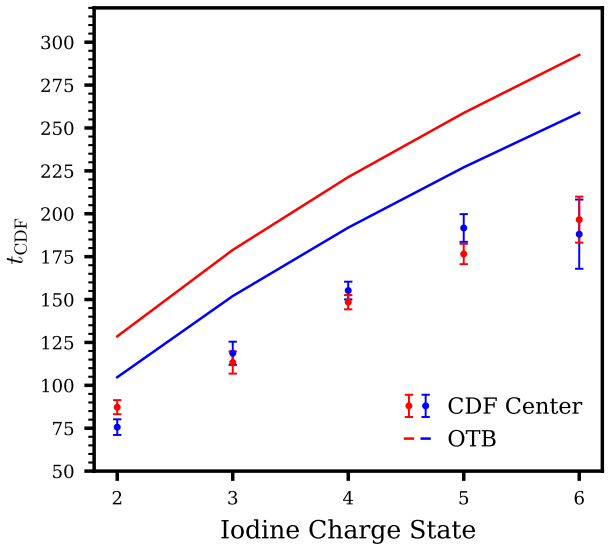

FIG. S6. Fitted time centres, t_{CDF}, from CDF fits to the low-momentum I^{n+} (n=2-6) yields from 1-IP (blue) and 2-IP (red). As described in the main text, comparison to a simple prediction from the classical OTB model are plotted as solid lines. Here, the data have not been subtracted by the value for I^{2+}.

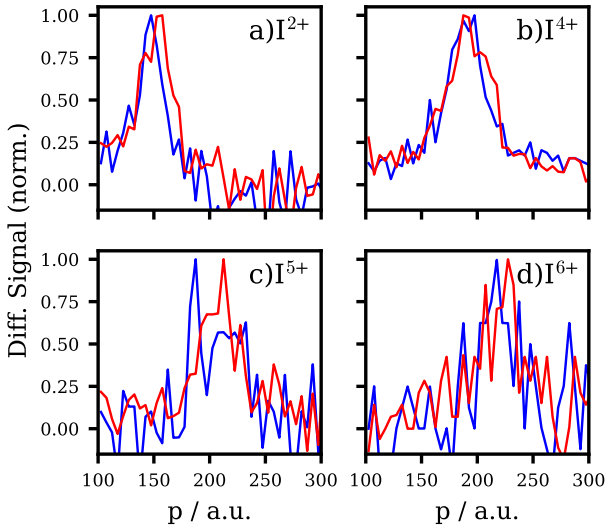

FIG. S7. Comparison of momentum distributions for Channel I I^{n+} ions (n=2,4,5,6) from 1-IP (blue) and 2-IP (red), obtained by integrating data between pump-probe delays of +0 fs and +300 fs, following subtraction of UV-late data (-300 fs to -100 fs).

higher momentum on average, but it is difficult to comment on the significance of this.

III. UV-INDUCED HI MODELLING

As discussed the main text, the modelling of the photoinduced HI elimination signatures in the I^+ ion, and the extraction of a branching ratio for this process, are dependent on the assumed KER distribution associated with the HI elimination step, and the KER of the subsequent Coulomb explosion of HI into H^+ + I^+. For 2-IP, the KER distribution associated with UV-induced HI elimination has been measured and reported recently [1], and so this was used in the modelling. No such distribution for the (potential/hypothetical) HI elimination channel from 1-IP has been reported, and so instead the KER distribution of the ground state I atom photodissociation channel from 1-IP was used. This is a reasonable approximation, given the reported KER distributions for HI elimination and ground state I atom dissociation in 2-IP closely resemble one another. However, to examine the role of the precise HI elimination KER distribution assumed, we also extracted branching ratios using the reported literature KER distribution for I* photodissociation from 1-IP[1]. We also explored the dependence of the extracted branching ratios on the precise KER distribution assumed for the HI Coulomb explosion step. These results are summarized in Table S1. It can be seen that these changes in the modelling have very minor effects on the branching ratios ultimately extracted.

One should also be aware of the caveats used in the present modelling and interpretation of the delay-dependent I^+ signals (which were only analysed in detail in light of the recent report of the HI elimination channel). For instance, the current analysis assumes that delay-dependent changes in the I^+ momentum distribution would occur only from depletion of XUV-only channels (Process 1) or from the Coulomb explosion of HI^{2+} (Process 2). This would exclude any possible signal from UV-induced C-I cleavage (to atomic iodine and propyl radical), followed by single valence ionization by the XUV pulse. This is justified on the basis that firstly the valence ionization cross-section is much smaller than the I 4d cross-section [5], and that any weak contribution from this process is expected to be similar between the two isomers. Similarly, the production of I^+ ions from Coulomb explosion of bound, but photoexcited molecules is neglected. This is reasonable as the potentials populated following single-photon UV absorption are directly dissociative along the C-I coordinate, and any contributions from potentially-bound Rydberg states populated by two-photon absorption are expect to be minor due to the low UV fluences adopted. Multiphoton dissociative ionization processes are also neglected. UV-only measurements show that firstly this is a very small channel, and more importantly, the I^+ ions produced predominantly have lower momenta than the regions-of-interest considered here. Finally, changes in the properties of the FEL pulses (e.g. total pulse energies) with pump-probe delay could yield changes in the shape of the I^+ momentum distribution, which could differ between the two datasets. As the datasets were recorded by rapidly and repeatedly scanning the pump-probe laser delay, we expect any potential drifts in the FEL conditions over acquisition time would be distributed fairly equally across the pump-probe delays. Additionally, measurements from an upstream pulse energy diagnostic show that, in the data recorded for both molecules, the mean FEL pulse energy is approximately constant (within a few percent) over the pump-probe delays considered.

One of the largest unknowns for the current modelling is how the propensity for Coulomb explosion into I^+ varies between parent molecule and the HI fragment under the employed XUV fluence. For the HI fragment, this is somewhat simplified as HI^{2+} is the only multiply charged state that can dissociate to yield I^+. Previous studies on the double ionization of HI have shown that the lowest-lying electronic states of the HI dication (with π^{-2} configurations) are stable with respect to dissociation [6, 7], reflecting a trend of increased stability as the HX^{2+} series is descended [8]. However, high-lying states (with $\pi^{-1}\sigma^{-1}$ and σ^{-2} configurations) are directly dissociative, yielding H^++I^+. We are unaware of detailed studies of the fragmentation dynamics of HI molecules following I 4d inner-shell ionization. However, we do note that reported HI AM spectra recorded at the I 4d pre-edge were dominated by the dissociative $\pi^{-1}\sigma^{-1}$ states [9] and these states are significantly populated in HBr following Br 3d ionization [10]. H^+ KE distributions from HBr^{2+} show significant contributions at ∼7 eV KER originating from these $\pi^{-1}\sigma^{-1}$ states [11]. Even if the dynamics following I 4d ionization were better understood for (cold, equilibrium) HI, the present

HI CE KER Distribution	2-IP (HI[1])	1-IP (I[1])	1-IP (I*[1])
μ=4 eV, σ=0.5 eV	5.5±1.2%	0.9±1.8%	0.9±1.7%
μ=4 eV, σ=1 eV	5.5±1.2%	0.9±1.8%	0.9±1.7%
μ=6 eV, σ=0.5 eV	5.9±1.3%	1.0±2.0%	0.9±1.7%
μ=6 eV, σ=1 eV	5.9±1.3%	1.0±2%	0.9±1.7%
μ=8 eV, σ=0.5 eV	6.4±1.4%	1.2±2.2%	1.0±1.8%
μ=8 eV, σ=1 eV	6.4±1.4%	1.2±2.2%	1.0±1.8%

TABLE S1. Comparison of extracted HI elimination branching ratios for different assumed KER distributions for UV-induced HI elimination and HI Coulomb explosion. The values highlighted in red text are those used in the main text.

case could however be complicated by the expected high degree of vibrational excitation in the HI photofragment [1]. For the 1- and 2-IP molecules, quantifying the branching ratios of the various fragmentation channels (from multiple parent charge states) yielding I^+ ions would be a very challenging task. For any given parent charge state populated, multiply fragmentation channels are possible, ultimately populating different iodine charge states [12, 13].

[1] M. A. Todt, S. Datta, A. Rose, K. Leung, and H. F. Davis, Subpicosecond HI elimination in the 266 nm photodissociation of branched iodoalkanes, Physical Chemistry Chemical Physics **22**, 27338 (2020).

[2] M. E. Corrales, V. Loriot, G. Balerdi, J. González-Vázquez, R. de Nalda, L. Bañares, and A. H. Zewail, Structural dynamics effects on the ultrafast chemical bond cleavage of a photodissociation reaction, Physical Chemistry Chemical Physics **16**, 8812 (2014).

[3] R. Forbes, F. Allum, S. Bari, R. Boll, K. Borne, M. Brouard, P. H. Bucksbaum, N. Ekanayake, B. Erk, A. J. Howard, *et al.*, Time-resolved site-selective imaging of predissociation and charge transfer dynamics: the CH_3I B-band, Journal of Physics B: Atomic, Molecular and Optical Physics **53**, 224001 (2020).

[4] F. Allum, Y. Kumagai, K. Nagaya, J. Harries, H. Iwayama, M. Britton, P. H. Bucksbaum, M. Burt, M. Brouard, B. Downes-Ward, *et al.*, Direct momentum imaging of charge transfer following site-selective ionization, Physical Review A **108**, 043113 (2023).

[5] T. N. Olney, G. Cooper, and C. Brion, Quantitative studies of the photoabsorption (4.5–488 ev) and photoionization (9–59.5 ev) of methyl iodide using dipole electron impact techniques, Chemical physics **232**, 211 (1998).

[6] L. Karlsson, S. Svensson, P. Baltzer, M. Carlsson-Gothe, M. Keane, A. N. de Brito, N. Correia, and B. Wannberg, The NVV Auger electron spectrum of the HI molecule, Journal of Physics B: Atomic, Molecular and Optical Physics **22**, 3001 (1989).

[7] M. Alagia, B. G. Brunetti, P. Candori, S. Falcinelli, M. Moix Teixidor, F. Pirani, R. Richter, S. Stranges, and F. Vecchiocattivi, The double photoionization of hydrogen iodide molecules, The Journal of Chemical Physics **124**, 204318 (2006).

[8] P. Candori, S. Falcinelli, F. Pirani, F. Tarantelli, and F. Vecchiocattivi, Interaction components in the hydrogen halide dications, Chemical physics letters **436**, 322 (2007).

[9] A. Pilcher-Clayton and J. H. Eland, Double photoionisation spectra of HI, CH_3I and CF_3I from TOF-PEPECO measurements, Journal of electron spectroscopy and related phenomena **142**, 313 (2005).

[10] B. Wannberg, S. Svensson, M. Keane, L. Karlsson, and P. Baltzer, Isotope effects in the auger electron spectra of hbr and dbr, Chemical Physics **133**, 281 (1989).

[11] A. Svensson, E. Hughes, A. Banichevich, S. Peyerimhoff, and B. Hess, Angular distribution of positive photofragments following dissociative double ionization in the hbr molecule, Journal of Physics B: Atomic, Molecular and Optical Physics **24**, 2997 (1991).

[12] J. W. McManus, T. Walmsley, K. Nagaya, J. R. Harries, Y. Kumagai, H. Iwayama, M. N. Ashfold, M. Britton, P. H. Bucksbaum, B. Downes-Ward, *et al.*, Disentangling sequential and concerted fragmentations of molecular polycations with covariant native frame analysis, Physical Chemistry Chemical Physics **24**, 22699 (2022).

[13] T. Walmsley, J. W. McManus, Y. Kumagai, K. Nagaya, J. Harries, H. Iwayama, M. N. Ashfold, M. Britton, P. H. Bucksbaum, B. Downes-Ward, *et al.*, The role of momentum partitioning in covariance ion imaging analysis, The Journal of Physical Chemistry A **128**, 4548 (2024).